CrossMark

A hybrid ensemble-OI Kalman filter for efficient data assimilation into a 3-D biogeochemical model of the Mediterranean

Kostas P. Tsiaras[1] · Ibrahim Hoteit[2] · Sofia Kalaroni[1] · George Petihakis[3] · George Triantafyllou[1]

Abstract A hybrid ensemble data assimilation scheme (HYBRID), combining a flow-dependent with a static background covariance, was developed and implemented for assimilating satellite (SeaWiFS) Chl-a data into a marine ecosystem model of the Mediterranean. The performance of HYBRID was assessed against a model free-run, the ensemble-based singular evolutive interpolated Kalman (SEIK) and its variant with static covariance (SFEK), with regard to the assimilated variable (Chl-a) and non-assimilated variables (dissolved inorganic nutrients). HYBRID was found more efficient than both SEIK and SFEK, reducing the Chl-a error by more than 40% in most areas, as compared to the free-run. Data assimilation had a positive overall impact on nutrients, except for a deterioration of nitrates simulation by SEIK in the most productive area (Adriatic). This was related to SEIK pronounced update in this area and the phytoplankton limitation on phosphate that lead to a built up of excess nitrates. SEIK was found more efficient in productive and variable areas, where its ensemble exhibited important spread. SFEK had an effect mostly on Chl-a, performing better than SEIK in less dynamic areas, adequately described by the dominant modes of its static covariance. HYBRID performed well in all areas, due to its "blended" covariance. Its flow-

dependent component appears to track changes in the system dynamics, while its static covariance helps maintaining sufficient spread in the forecast. HYBRID sensitivity experiments showed that an increased contribution from the flow-dependent covariance results in a deterioration of nitrates, similar to SEIK, while the improvement of HYBRID with increasing flow-dependent ensemble size quickly levels off.

Keywords Data assimilation · Biogeochemical model · Kalman filter · Ocean color · Mediterranean

Responsible Editor: Dieter Wolf-Gladrow

✉ Kostas P. Tsiaras
ktsiaras@hcmr.gr

[1] Hellenic Centre for Marine Research, Anavyssos, P.O. Box 712, 19013 Attica, Greece

[2] King Abdullah University of Sciences and Technology, Thuwal, Saudi Arabia

[3] Hellenic Centre for Marine Research, P.O. Box 2214, 71003 Iraklio, Greece

1 Introduction

The Mediterranean is a semi-enclosed sea, connected to the Atlantic Ocean through the Strait of Gibraltar in the west and to the Sea of Marmara and the Black Sea through the Dardanelles Straits in the northeast (Fig. 1). Its pelagic ecosystem may be characterized as oligotrophic, exhibiting a well-defined eastward decreasing trend in primary productivity (Moutin and Raimbault 2002) that is related to the anti-estuarine circulation at Gibraltar, with inflowing nutrient poor surface Atlantic waters and outflowing subsurface Mediterranean waters. The eastern basin, separated by the shallow Sicily Strait (~500 m), is recognized as one of the most oligotrophic areas in the world (Azov 1991). Phosphorous is the limiting nutrient for phytoplankton and bacterial growth, with decreasing concentrations from west to east (Krom et al. 2004). The primary production is mainly controlled by vertical mixing processes that supply the euphotic zone with deep water nutrients, reaching its maximum between December and April and minimum between June and September. The seasonal cycle is stronger in areas characterized by deep water formation, such as the Gulf of Lions in the northwestern Mediterranean, which is one of the most productive areas in the Mediterranean (Morel et al. 1991; Bosc et al. 2004).
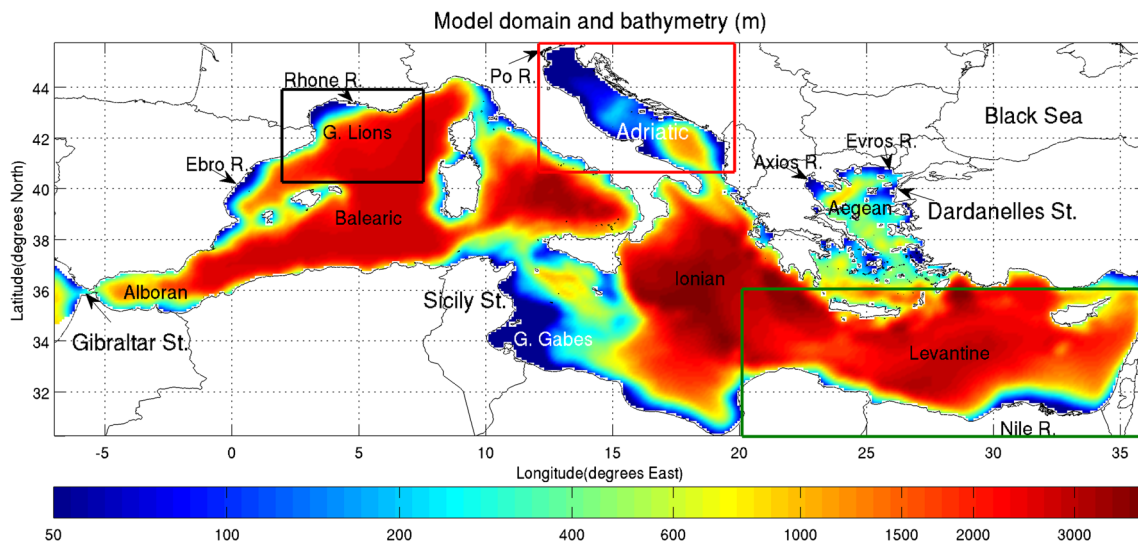
Model domain and bathymetry (m)

Fig. 1 Mediterranean model domain and bathymetry (m). Major rivers and straits are indicated, along with the Gulf of Lions (*black box*), Adriatic Sea (*red box*), and Levantine basin (*green box*), where averages are calculated in Figs. 5, 7, and 8

Relatively increased productivity is also found in areas receiving river nutrient inputs (Fig. 1), such as the Northern Adriatic, the North Aegean, and the Gulf of Lions.

Numerical models are now routinely used to simulate the dynamics of marine ecosystems, which are subject to changes from climate and human pressures, providing a valuable tool for the management of marine resources. However, the models ability to accurately simulate the space-time variability of the marine environment is limited by various sources of uncertainties, such as those of model structure and parameterization, as well as the quality of initial conditions and meteorological forcing. In this respect, the pronounced characteristics of the Mediterranean ecosystem, such as the P-limited oligotrophism and the role of the physics as the main driver on the ecosystem processes, significantly add to the complexity. Data assimilation is a process of nudging the model simulations toward available observations to reduce the uncertainties in the model outputs. This approach is widely used in atmospheric and ocean sciences and has also become popular in biogeochemical ocean applications in the last decades (see review in Edwards et al. 2015). Particularly in the Mediterranean Sea, biological data assimilation has been applied regionally in the Ligurian Sea (Lenartz et al. 2007; Kalaroni et al. 2016), the Northwest coast of Spain (Torres et al.2006), the Cretan Sea (Allen et al. 2003; Hoteit et al. 2003, 2004; Triantafyllou et al. 2003, 2007, 2012; Kalaroni et al. 2016), and at basin scale (Hoteit et al. 2005; Teruzzi et al. 2014).

Ensemble Kalman filters (EnKFs) are currently among the most popular data assimilation techniques due to their efficiency and robustness in dealing with large scale nonlinear systems and their reasonable computational cost. Different types of EnKFs are now commonly used for physical (e.g., Hoteit et al. 2002; Evensen 2003; Nerger et al. 2006; Xu et al. 2013; Hoteit et al. 2013; Hoteit et al. 2005) and biochemical

(Natvik and Evensen 2003; Triantafyllou et al. 2003; Nerger and Gregg 2007; Simon and Bertino 2009; Ciavatta et al. 2011, 2014; Hu et al. 2012;) ocean applications.

In an EnKF, the distribution of the state of the system, conditioned on available observations, is represented by a set of state vectors called ensemble. The standard forecast-update steps of the Kalman filter are then implemented as follows. The ensemble members are first propagated in time with the model to estimate the forecast and its error covariance as the sample mean and covariance of the forecasted members. These are then used in the Kalman correction step to update the forecast with the incoming observations. In practice, a sufficiently large, but computationally demanding, ensemble is needed to well describe the state distribution (Pham 2001; Song et al. 2010). A small ensemble may result in an underestimation of the state variance and a degenerative analysis, characterized by an ensemble collapse (Whitaker and Hamill 2002). This limitation is often mitigated by introducing appropriate inflation and localization (Edwards et al. 2015). Another approach that was proven efficient for enhancing the performance of the EnKF when implemented with small ensembles is the so-called hybrid scheme (Hamill and Snyder 2000). It combines the error covariance estimated from an EnKF ensemble with a pre-selected static background error covariance representing the climatology of the system statistics (Hamill and Snyder 2000; Song et al. 2010; Lui et al. 2016). The hybrid method was found particularly efficient when the filter is implemented with a small ensemble and also in the presence of model error (Wang et al. 2008; Counillon et al. 2009; Song et al. 2010).

Hybrid assimilation schemes have been successfully applied in meteorology (e.g., Hamill and Snyder 2000; Etherton and Bishop 2004; Wang et al. 2008) and more

recently in ocean forecasting (Counillon et al. 2009) and sub-surface flows (Gharamti et al. 2014). In the present study, a hybrid scheme was developed and implemented for efficient data assimilation into a marine ecosystem model of the Mediterranean Sea. The scheme combines the ensemble-based forecast error covariance of the singular evolutive interpolated Kalman (SEIK, Pham 2001) filter, with a static

background covariance built from a set of empirical orthogonal functions (EOFs), as in the singular fixed extended Kalman (SFEK, Hoteit et al. 2002). The hybrid algorithm was implemented and tested for assimilation of satellite Chl-a data into a three-dimensional ecosystem model of the Mediterranean. Data assimilation for marine ecosystems can be quite challenging, given the large number of state variables and the required computational cost, the short time-scales, and nonlinear nature of biogeochemical processes (Edwards et al. 2015). In particular, for the shelf and regional areas of Mediterranean ecosystems, these shortcomings have been analyzed and discussed in the works of Triantafyllou et al. (2007) and Triantafyllou et al. (2005), supporting the idea of the development of a more efficient Kalman scheme. The main aim of this study is to assess the performance of the new hybrid scheme for data assimilation and to test its efficiency and robustness before implementing it operationally as part of the POSEIDON forecasting system (www.poseidon.hcmr.gr).

The paper is organized as follows. Section 2 briefly describes the coupled hydrodynamic/biogeochemical model. Section 3 presents the ensemble hybrid data assimilation scheme. Section 4 assesses the performance of the new hybrid scheme against SEIK and SFEK, first with regard to the assimilated data (Chl-a) and then with regard to non-assimilated model variables, such as dissolved inorganic nutrients. In section 5, the performance of the assimilation schemes is discussed in relation to the ensemble spread and forecast update. The performance of the hybrid scheme is also further analyzed through a series of sensitivity experiments, to investigate the effect of the dynamic ensemble size and the blending parameter. Concluding remarks are offered in section 6.

2 Materials and methods

2.1 Model description

A three-dimensional coupled hydrodynamic/biogeochemical model is implemented at Mediterranean basin scale (Fig. 1). The coupled model is comprised of the Princeton Ocean Model (POM, Blumberg and Mellor 1983) and the European Regional Seas Ecosystem Model (ERSEM, Baretta et al. 1995). POM is a primitive equation, free-surface, and sigma-coordinate model that employs a 2.5 turbulence closure scheme (Mellor and Yamada 1982) to compute vertical viscosity/diffusivity. It is a widely spread community

model (www.ccpo.odu.edu/POMWEB) with numerous applications in coastal and open ocean studies, including the Mediterranean (Zavatarelli and Mellor 1995; Horton et al. 1997; Korres and Lascaratos 2003), among others. ERSEM is a comprehensive generic biogeochemical model that has been successfully implemented in various coastal and open sea ecosystems, such as the North Sea (Pätsch and Radach 1997), the oligotrophic Mediterranean (Allen et al. 2002; Petihakis et al. 2002), and the Arabian Seas (Blackford and Burkill 2002; Triantafyllou et al. 2014), among others. It follows the functional group approach, adequately describing the pelagic plankton food web with four phytoplankton groups (diatoms, nanoplankton, picoplankton, and dinoflagellates), three zooplankton groups (heterotrophic nanoflagellates, microzooplankton, and mesozooplankton), and bacteria. Its variables also include dissolved and particulate organic matter, along with dissolved inorganic nutrients (phosphate, nitrate, ammonium, and silicate), while carbon dynamics are loosely coupled with nitrogen and phosphorus dynamics, as plankton groups have dynamically varying C:N:P internal pools (in total, 38 pelagic variables are prognostically computed). We refer the reader to Petihakis et al. (2002), Tsiaras et al. (2014), and Petihakis et al. (2014) for more details on the biogeochemical model description and implementation.

The coupled hydrodynamic/biogeochemical model is currently operational in the Mediterranean, providing 4-day forecasts (without data assimilation) for dissolved inorganic nutrients, plankton biomass, and production, as part of the POSEIDON forecasting system (www.poseidon.hcmr.gr; Korres et al. 2007; Tsiaras et al. 2010). It successfully reproduces the main features of the Mediterranean ecosystem, such as the east-west gradient of productivity and phosphorus limitation, the seasonal cycle of plankton production that is controlled by vertical mixing processes, and the increase of productivity in coastal areas receiving river nutrient inputs (Tsiaras et al. 2010).

In this study, simulations were performed for year 2000, and the atmospheric forcing was obtained from the POSEIDON operational weather forecast (Papadopoulos et al. 2002). Fresh water discharge and nutrient inputs from (25) major rivers in the Mediterranean were obtained from hydrological/nutrient emission modeling of the Mediterranean drainage basin (Ludwig et al. 2009). Open boundary conditions near the Gibraltar strait (Fig. 1) were obtained from available climatologies for dissolved inorganic nutrients (MEDATLAS 2002, www.ifremer.fr/medar/) and temperature/salinity (MODB-MED4), while radiation conditions were adopted for current velocities. The Dardanelles water exchange, an important mechanism for the ecosystem of the Aegean Sea (Petihakis et al. 2014), is parameterized through a two-layer open boundary condition (Nittis et al. 2006), with prescribed climatological data of seasonally varying water inflow and dissolved inorganic nutrients (Tugrul et al. 2002).

2.2 Observational dataset

Assimilated observations consist of remote sensing Chl-a, retrieved by SeaWiFS (Sea-viewing Wide Field-of view Sensor) and processed using the Ocean Chlorophyll 4-version 4 (OC4-v4) algorithm (O'Reilly et al. 1998). The SeaWiFS data are 8-day composite products (9×9 km^2 resolution) for year 2000. On top of assessing the performance of the different filters in improving the model Chl-a estimate, we also evaluated the filters in term of their impact on non-assimilated variables, such as dissolved inorganic nutrients that are primary constituents in the biogeochemical model dynamics. For that purpose, given the limited data availability on specific years, a seasonal "climatology" of near-surface (0–50 m) in situ data was constructed, by aggregating available observations in the Mediterranean on different seasons over 1990–1999 period, obtained from the SeaDataNet database (www.seadatanet.org). The simulated seasonal mean phosphate and nitrate concentrations, extracted at the data locations, were compared against the observations on different seasons. The model performance, particularly the efficiency of data assimilation in reproducing the nutrients spatial/seasonal variability, was assessed by calculating the following model skill indexes over all model (M)/data (D) pairs (n) (e.g., Stow et al. 2009; Jolliff et al. 2009):

- Percentage model bias PBIAS $= \left(\sum (D-M) / \sum D \right)^* 100$,

which computes the percentage normalized difference between the model and data mean. It basically evaluates whether the model systematically underestimates or overestimates the observations.

- Pearson correlation coefficient PCC

$$= \sum \left(D - \overline{D} \right) \cdot \left(M - \overline{M} \right) / \sqrt{ \sum \left(D - \overline{D} \right)^2 \cdot \left(M - \overline{M} \right)^2 },$$

where over-bar denotes a mean value. This provides a measure of whether the model is able to reproduce the observed spatial variability. $PCC = 1$ indicates a perfect correlation.

- RMS model error $RMSE = \sqrt{ \sum (D-M)^2 / n }$,

which gives the overall goodness of fit between model and data values, with $RMSE = 0$ indicating a perfect fit.

- Normalized standard deviation NSTD

$$= \sigma^2(M) / \sigma^2(D),$$

which measures whether the model exhibits a similar overall variability to the observed (NSTD = 1).

3 The hybrid SEIK filter

The hybrid ensemble scheme proposed in this study uses a combination of covariances from the singular extended interpolated Kalman (SEIK; Pham 2001) and the singular fixed extended Kalman (SFEK, Hoteit et al. 2002; Hoteit and Pham 2004) in the Kalman update step. SFEK uses a static background covariance, built from a set of EOFs, while SEIK employs a flow-dependent error covariance, estimated from a stochastically generated ensemble (Hoteit et al. 2012). HYBRID bears some similarities with the singular semi-evolutive interpolated Kalman (SSEIK, Hoteit et al. 2002), in the sense that its algorithm also involves static and flow-dependent covariances. In SSEIK, however, only a "part" of the filter covariance is integrated in time with the model during the forecast step through a well-chosen reduced ensemble that is sampled, at every analysis step, based on certain criteria (as for example propagating the part of the covariance that represents the dominant error modes as extracted by a singular value decomposition, SVD).

3.1 SEIK filter

SEIK operates as a succession of three consecutive steps: a sampling step to generate the ensemble from the filter's estimate and its covariance, a forecast step to integrate the ensemble forward with the model, and a Kalman update step of the forecast ensemble mean and covariance with the incoming observations.

3.1.1 Sampling step

Starting from an available analysis state and a low rank (r) error covariance $P^a(t_k) = L_k U_k L_k^T$ at a given time t_k, an ensemble of $N = r + 1$ states $X_1^a(t_k), \ldots, X_N^a(t_k)$ is randomly drawn after every assimilation cycle (t_k) in such a way that their sample mean and covariance exactly match $X^a(t_k)$ and $P^a(t_k)$ (Note that $N = r + 1$ is the smallest ensemble that could be generated to describe a rank-r covariance matrix, Pham 2001) i.e.,

$$X^a(t_k) = \frac{1}{N} \sum_{i=1}^{N} X_i^a(t_k), \tag{1}$$

$$P^a(t_k) = \frac{1}{N} \sum_{i=1}^{N} \left[X_i^a(t_k) - X^a(t_k) \right] \left[X_i^a(t_k) - X^a(t_k) \right]^T \tag{2}$$

U_k is a $r \times r$ matrix and L_k is the so-called filter correction basis of dimension $n \times r$, with n being the size of the system

state $X(t_k)$. To generate $X_i^a(t_k)$, one may use the second-order exact sampling technique (Pham 2001; Hoteit et al. 2002), in which the ith ensemble member is computed as

$$X_i^a(t_k) = X^a(t_k) + \sqrt{r+1}\, L_k \left(\Omega_{k,i} C_k^{-1} \right)^T, \qquad (3)$$

where C is the square root matrix of U_k (that can be obtained by Cholesky decomposition) and $\Omega_{k,i}$ denotes the ith row of a randomly generated matrix Ω_k, with columns orthonormal and orthogonal to the vector $[1 \cdots 1]^T$, so that the $X_i^a(t_k)$ satisfy (1) and (2).

3.1.2 Forecast step

The generated ensemble members $X_i^a(t_k)$ are propagated forward with the model (M), to compute the forecast ensemble $X_i^f(t_{k+1}) = M(t_{k+1}, t_k) X_i^a(t_k)$. The forecast state $X^f(t_{k+1})$ and its error covariance matrix $P^f(t_{k+1})$ are then estimated as the sample mean and covariance of the $X_i^f(t_{k+1})$, respectively. One can then decompose $P^f(t_{k+1})$ as

$$P^f(t_{k+1}) = L_{k+1} \left[NTT^T \right]^{-1} L_{k+1}{}^T, \qquad (4)$$

with

$$L_{k.} = \left[X_1^f(t_k),\ \ldots,\ X_{r+1}^f(t_k) \right] \cdot T \qquad (5)$$

and T is a $(r+1) \times r$ orthogonal matrix with zero column sums (Hoteit et al. 2002).

3.1.3 Analysis step

Once a new observation y_{k+1} becomes available, the forecast and its error covariance matrix are updated exactly as in the Kalman filter, as

$$X^a(t_{k+1}) = X^f(t_{k+1}) + K_{k+1} \left[y_{k+1} - H_{k+1} \left(X^f(t_{k+1}) \right) \right] \qquad (6)$$

$$P^a(t_{k+1}) = L_{k+1} U_{k+1} L_{k+1}{}^T, \qquad (7)$$

where K_{k+1} is the so-called Kalman gain, given by

$$K_{k+1} = L_{k+1} U_{k+1} (HL)_{k+1}^T R_{k+1}^{-1} \qquad (8)$$

$$(HL)_{k+1} = \left[H_{k+1} \left(X_1^f(t_{k+1}) \right), ..., H_{k+1} \left(X_{r+1}^f(t_{k+1}) \right) \right] \cdot T, \qquad (9)$$

with H_{k+1} the observational operator at time t_{k+1}, practically computing the predictions of the observation by the forecast

members. R_{k+1} is the observational error covariance, and U_{k+1} is the computed from

$$U_{k+1}^{-1} = \rho \frac{1}{N} \left(T^T T \right)^{-1} + (HL)_{k+1}^T R_{k+1}^{-1} (HL)_{k+1}. \qquad (10)$$

ρ is the so-called "forgetting" factor, taking values between 0 and 1. It is used to inflate the error covariance (by $1/\rho$) to account for the various sources of errors, assigning more or less confidence on the observations in relation to the model forecast (Hoteit, Pham and Blum 2002).

Localization is applied as described by Nerger et al. (2006) to filter out long-range spurious correlations and to allow more degrees of freedom to fit the data. This is implemented in practice by updating the model state variables at each grid cell using only observations within a specified cutoff radius.

3.2 SFEK filter

The update step of the SEIK filter is only applied along the directions of L_k, which was hence called correction basis of the filter (Pham 2001). L_k is updated in time to follow changes in the system dynamics, but this can be computationally demanding. Noticing that the filter generally behaves well when the update step is always applied along an initial correction basis L_0 described by a set of EOFs computed from a historical model trajectory, Hoteit et al. (2002) suggested to keep L_0 invariant with time to drastically reduce the computational load. In the resulting SFEK filter, the forecast step only computes the forecast state, by integrating the analysis state with the model $X^f(t_{k+1}) = M(t_{k+1}, t_k) X^a(t_k)$. L_k is kept invariant equal to L_0, and U_k is still updated as in Eq. 10. The analysis step is then identical to that of SEIK filter (Eqs. 6–8).

3.3 HYBRID filter

The HYBRID scheme uses a weighted combination of the (low-rank and already scaled/inflated) covariances of SEIK and SFEK, following the formulation of Hamill and Snyder (2000). More specifically, HYBRID uses

$$P_{k+1}{}^{\text{Hybrid}} = (1-\alpha) \cdot P_{k+1}{}^{\text{SEIK}} + \alpha \cdot P_{k+1}{}^{\text{SFEK}} \qquad (11)$$

as background covariance in the SEIK filter update step, where α is the weighting factor between 0 and 1. Based on the low-rank decomposition of P^{SEIK} and P^{SFEK}, one can write:

$$P_{k+1}^{\text{Hybrid}} = (1-\alpha)\cdot L_{k+1}^{\text{SEIK}}\left[NT^TT\right]^{-1}\left(L_{k+1}^{\text{SEIK}}\right)^T + \alpha\cdot L^{\text{SFEK}}U_k^{\text{SFEK}}\left(L^{\text{SFEK}}\right)^T,$$

$$= \left[L_k^{\text{SEIK}}|L^{\text{SFEK}}\right]\cdot\begin{bmatrix}(1-a)\cdot(NT^TT)^{-1} & 0 \\ 0 & a\cdot U_k^{\text{SFEK}}\end{bmatrix}\cdot\left[L_k^{\text{SEIK}}|L^{\text{SFEK}}\right]^T$$

$$= L_k^{\text{Hybrid}}U_k^{\text{Hybrid}}\left(L_k^{\text{Hybrid}}\right)^T,$$

$$(12)$$

which can be then directly used in Eqs. 6–10 to update the forecast with a blended correction basis of flow-dependent and climatological (static) directions.

For resampling, we follow Wang et al. (2008) and generate the analysis ensemble from the analysis covariance of the flow-dependent part only, that is we use Eq. 3 with $L_k = L_k^{SEIK}$ and C_k^{-1} the cholesky decomposition of U_k^{SEIK}, with:

$$\left(U_{k+1}^{\text{SEIK}}\right)^{-1} = \rho\frac{1}{N}\left(T^TT\right)^{-1}$$
$$+ \left(HL^{\text{SEIK}}\right)_{k+1}^T R_{k+1}^{-1}\left(HL^{\text{SEIK}}\right)_{k+1}. \quad (13)$$

This ensemble is then integrated with the model as in SEIK to compute the forecast state, as the mean of the forecasted members and P_{k+1}^{SEIK} as their sample covariance. In terms of computational load, the size of the flow-dependent ensemble in the hybrid scheme can be significantly smaller than that of the SEIK filter, meaning important savings in computing hours.

4 Experiments design and results

The model state vector consists of all (38) pelagic variables of the biogeochemical model (see model description section 2.1). The initial/static correction basis L_0 was generated by performing an EOF analysis on a long-sequence of (bi-daily) model outputs, simulated over a 2-year period (January 1997–December 1998). A set of 25 EOF modes was retained, as described by Hoteit et al. (2001), to form the initial correction basis, explaining about 84% of the system's variance.

The observation error was estimated as 20% of the SeaWiFS Chl-a, i.e., $R(i,j) = [0.2 \times Chl\text{-}a_{SeaWiFS}(i,j)]^2$, assuming a 20% measurement error. This is lower from the SeaWiFS errors that are usually used in the literature (~35%). A recent work that sampled a great variety of the Atlantic waters (including temperate environments) reported an accuracy of 16% (Brewin et al. 2016). In this preliminary study, testing the efficiency of the proposed ensemble hybrid scheme for data assimilation into a marine ecosystem model, the specified 20% mean error was considered as a compromise between coastal (higher error) and open sea (lower error) areas. More sophisticated approaches for estimating the observation error have been recently proposed to tackle this challenging issue in data assimilation (e.g., Luo and Bhakta 2016; Miyoshi et al. 2013). Moreover, advanced techniques have been suggested

for the online estimation of the observation noise variance as hyper-parameters during the filtering process (e.g., Ueno and Nakamura 2014; Dreano et al. 2017; Li et al. 2009). These would still however require limiting the spatial variability of the observational error variance through some kind of parameterization in order to reduce the number of hyper-parameters to be estimated.

A cutoff radius of ~30 km was adopted for the localization of the filter update. This was chosen by trial-and-error, after a series of sensitivity experiments testing the impact of various values on the performance of the filtering schemes. Consistent with Hamill et al. (2001), we found that a small cut-off radius was more suitable when the filter is implemented with small ensembles. SEIK performance was slightly improved with a slightly larger (~60 Km) cut-off radius. The ensemble size of SEIK is $N = 26$, while the size of the HYBRID flow-dependent ensemble is $N_D = 10$. The rank of the static background covariance in HYBRID and SFEK is $r_1 = 16$ and $r_0 = 25$, respectively (see Table 1). The SeaWiFS 8-day average Chl-a is assimilated at the middle of the 8-day assimilation window (end of day 4). The filter performance in improving the model Chl-a estimate is evaluated comparing the model 8-day average Chl-a of analysis and forecast states against the respective assimilated SeaWiFS 8-day average Chl-a (Figs. 2–5). This model 8-day average is computed as the average of the analyzed Chl-a at day 4 and the forecasted Chl-a on the remaining 7 days, considered as the best estimate of the 8-day average Chl-a data over the assimilation window.

Various sensitivity experiments were performed to set the SEIK/HYBRID ensemble ranks (r_k, r_0), forgetting factors (ρ), and the covariances weighting factor (α). The best parameters were chosen, based on the filters performance in estimating Chl-a, as well as the system robustness and behavior with non-assimilated variables (dissolved inorganic nutrients). The

**Table 1** Attributes of different assimilation experiments

Scheme	Flow-dependent ensemble size (N/N_D)	Rank of static covariance (r_1/r_0)	Forgetting factor (ρ)	Hybrid weighting factor (a)
SEIK	26	–	0.4	–
SFEK	–	25	0.85	–
HYBRID_REF	10	16	0.85	0.95
HYBRID_0.7	10	16	0.85	0.7
HYBRID_0.5	10	16	0.85	0.5
HYBRID_5	5	21	0.85	0.95
HYBRID_15	15	11	0.85	0.95
HYBRID_20	20	6	0.85	0.95

attributes of the selected data assimilation experiments are summarized in Table 1. The performance of HYBRID was compared with that of SEIK and SFEK. Results of sensitivity experiments to test the HYBRID performance with different values of the weighting factor (α) and the size of the dynamic ensemble (see Table 1) are also presented and discussed.

4.1 Impact of data assimilation on Chl-a

The performance of the HYBRID scheme is first evaluated against the assimilated SeaWiFS Chl-a, and in comparison with SEIK, SFEK and a model free-run without assimilation. Two examples illustrating the impact of data assimilation with the HYBRID scheme on the model Chl-a are shown in Fig. 2 for spring and summer periods. During April, the model free-run underestimates the phytoplankton spring bloom in the Gulf of Lions (see Fig. 1). This bloom is triggered by an increased vertical mixing in this dense water formation site, which results in the entrainment of deep water nutrients in the euphotic zone (e.g., Marty et al. 2002). The model free-run partly reproduces such a bloom in early March (not shown), but underestimates the late April bloom that is captured by
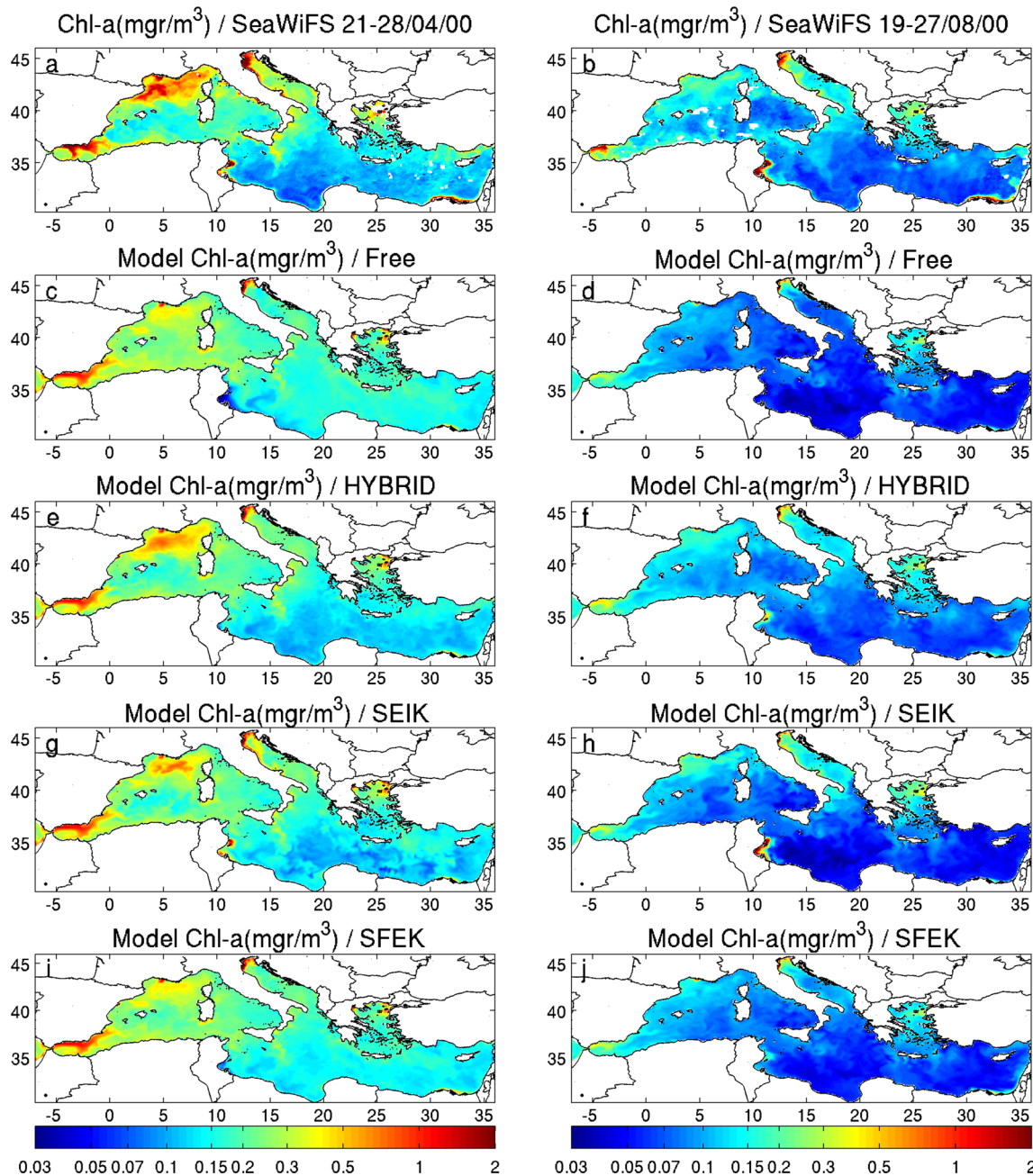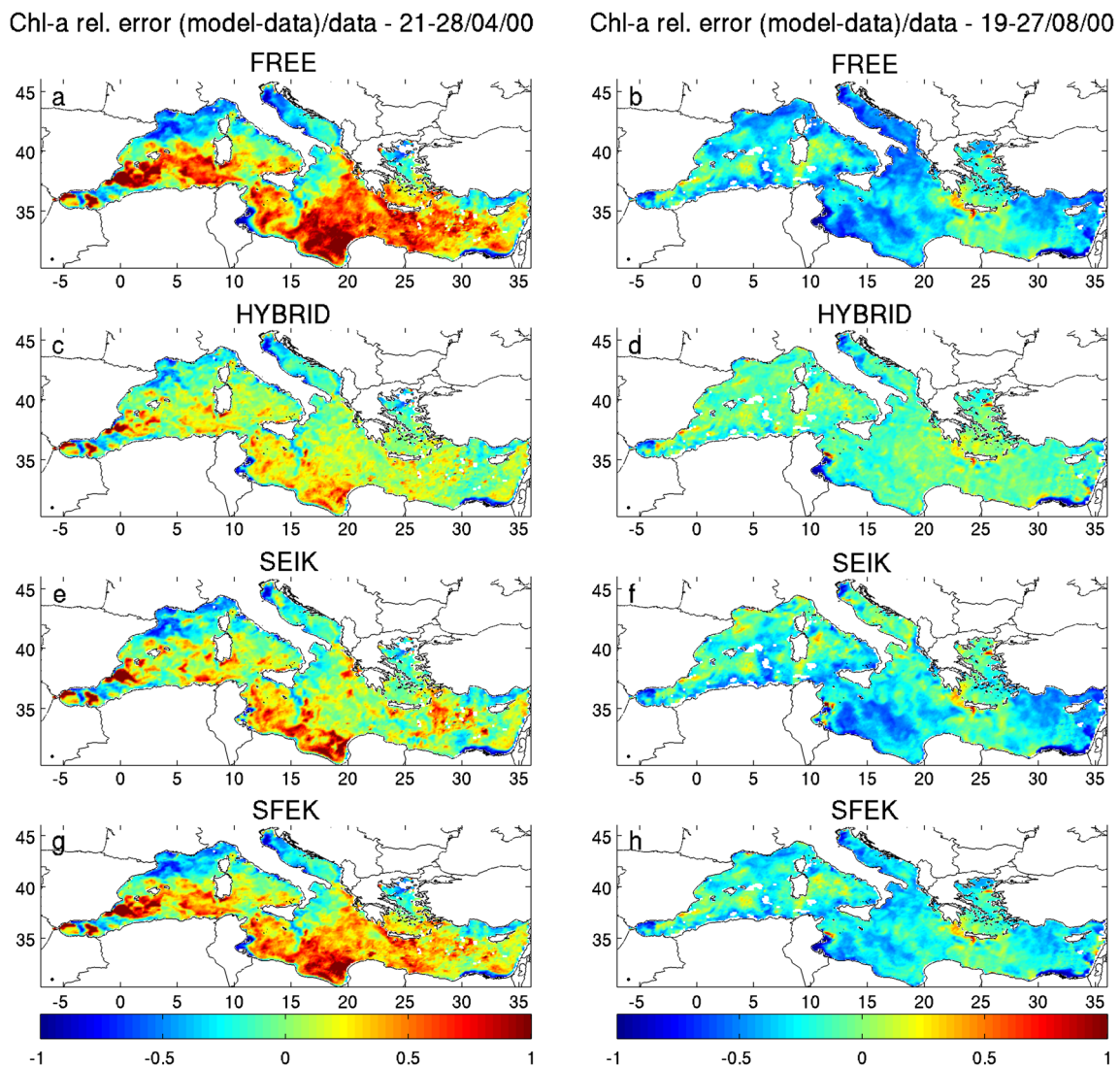

Fig. 2 Model simulated Chl-a without assimilation (FREE) and with the different filter schemes (HYBRID, SEIK, SFEK) against SeaWiFS Chl-a for 21-28/04/2000 (left) and 19-27/08/2000 (right)

SeaWiFS. This underestimation is significantly reduced after assimilation, particularly using HYBRID and SEIK, and somewhat less with SFEK. This is better depicted in Fig. 3, plotting the relative differences between the simulated and SeaWiFS Chl-a. Another area of model deficiency is the overestimation of Chl-a in the Eastern Levantine, Ionian, and Balearic Seas (see Fig. 1), which is mostly related to the hydrodynamic model overestimation of winter-spring vertical mixing. Again, this is significantly improved in HYBRID, SEIK, and to a lesser degree in SFEK. During August, the free-run Chl-a is underestimated, mainly in the Adriatic and N. Aegean, the Gulf of Lions, and some areas in the Ionian and Eastern Levantine. This bias is practically corrected (Figs. 2 and 3) over most of the domain by the HYBRID scheme. Few exceptions are some coastal areas in the Northern Adriatic, the Gulf of Gabes, where the retrieved Chl-a by the satellite bio-optical algorithm may be

overestimated due to direct bottom reflection in shallow waters (Barale et al. 2008) and the Egyptian coast that is influenced by nutrient inputs from the River Nile (Fig. 1). SEIK achieves a slightly better performance in the Adriatic, as compared to HYBRID. It also behaves better than SFEK in the Gulf of Lions and the N. Aegean Sea, but is slightly less efficient in some other areas in the South Ionian and the Eastern Levantine.

Figure 4 plots the annual mean fractional change of HYBRID, SEIK, and SFEK Chl-a relative error with respect to the free-run error, illustrating the overall performance of the different schemes throughout the Mediterranean. HYBRID reduces the estimation error by more than 40% in most areas compared to the free-run. Slightly less improvement is achieved in more productive areas, receiving important lateral nutrient inputs, such as the Northern Adriatic (River Po), the Gulf of Lions (River Rhone), the Northern Aegean (river and
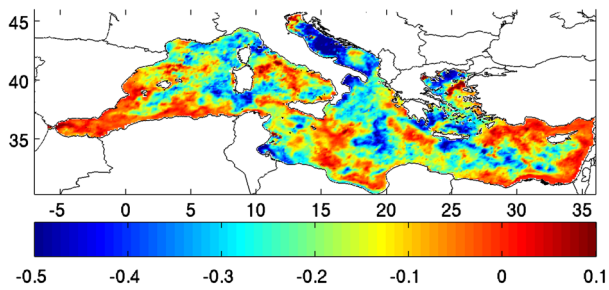

Fig. 3 Model simulated Chl-a relative error (model-SeaWiFS)/SeaWiFS, without assimilation (FREE) and with the different filter schemes (HYBRID, SEIK, SFEK), during 21-28/04/2000 (*left*) and 19-27/08/2000 (*right*)
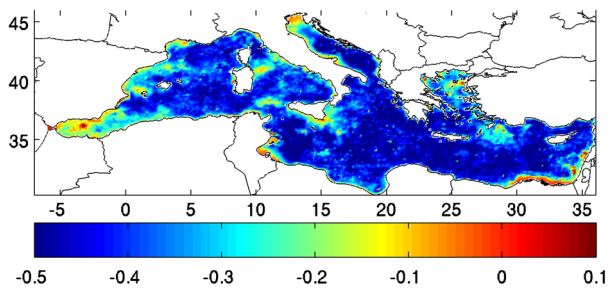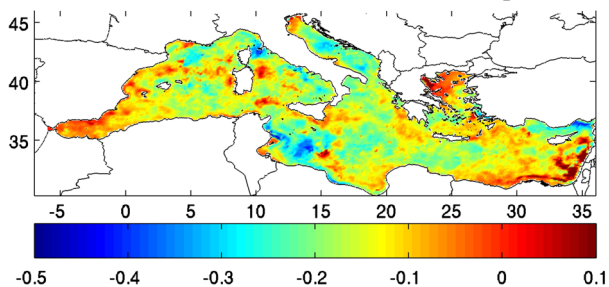
Fig. 4 Fractional change of the annual mean Chl-a relative error (|data-model|/data) against the SeaWiFS Chl-a, over the free run simulation (ASSIM/FREE-1) for the simulations adopting the HYBRID (*top*), SEIK (*middle*), and SFEK (*bottom*) assimilation filter schemes

Black Sea Water inputs), and the Nile area, or exhibiting strong space-time variability, such as the Alboran Sea. The latter is characterized by important dynamical variations of the circulation driven by the Atlantic water inflow and local atmospheric forcing (e.g., Macias et al. 2014). SFEK reduction of the estimation error exhibits a similar pattern but to a much less degree, as compared to HYBRID. This could be attributed to the spatial variability of the assigned observation error, which was estimated as a function of satellite Chl-a, resulting in a relatively weaker correction in more productive areas where observations are considered more uncertain, thus, receiving less weight in the filter update. SEIK exhibits somehow a different behavior, being more efficient in more productive areas, such as the Adriatic, the Gulf of Lions, and the North Aegean and less efficient in others, mostly open-sea areas in the Eastern Levantine and the southwestern Mediterranean. This is due to the nature of its fully flow-dependent ensemble, exhibiting more spread in the more productive areas. Overall, SEIK provides a mixed performance,

showing a better behavior than SFEK in some areas and worse in others, while both being significantly less performant than HYBRID in most areas.

The seasonal variability of the relative Chl-a error over different areas of the Mediterranean is shown in Fig. 5. We focus on the Adriatic Sea, because it represents a river-influenced productive area, the Gulf of Lions, because it is a dynamically varying area that exhibits a strong spring bloom, and the Levantine area that is a more oligotrophic area. HYBRID outperforms both SEIK and SFEK throughout the year in all areas, except in the Adriatic, where SEIK performs better over most of the year. SEIK is also slightly better than SFEK in the Gulf of Lions, but worse in the Levantine area during the summer-autumn period. Overall, SEIK appears to perform better than SFEK during winter-spring period that is characterized by stronger variability, while SFEK is slightly better during the calmer summer-autumn period. SEIK provides a slightly lower mean 8-day estimation error (0.34) in the Mediterranean, as compared to SFEK (0.343). One can notice that despite this, SEIK leads to a slightly worse Mediterranean average analysis and forecast errors (Fig. 5), as compared to SFEK. This is related to the stronger impact of SEIK on non-assimilated variables, such as dissolved inorganic nutrients that results in a more efficient decrease of the Chl-a error over the 8-day period (see discussion in section 5.1). Furthermore, HYBRID appears very efficient in the forecast update, as depicted by its very low analysis error, as compared to both SEIK and SFEK. This is not reflected in its forecast error, being much closer to the other schemes, but gives HYBRID an important "head start" over the other schemes, which results in a significantly lower error on the 8-day period.

Comparing other skill indexes (Table 2), SEIK achieves better scores in terms of overall percentage bias, RMS error and standard deviation, as compared to both HYBRID and SFEK, which is mainly due to its stronger impact in the most productive Adriatic area. On the other hand, HYBRID estimates correlate better with the data.

4.2 Impact on non-assimilated variables

The impact of data assimilation on model predicted dissolved inorganic nutrients (phosphate, nitrate) in terms of bias, correlation, standard deviation, and RMS error, against observations obtained from the SeaDataNet seasonal climatology (1990–1999) is outlined in Table 2. The free-run shows an overall underestimation (positive percentage model bias, PBIAS) for both nitrates and phosphates, and also a weaker phosphate variability (normalized STD < 1), as compared to the observed. SEIK achieves the stronger decrease of PBIAS and increase of STD for phosphate concentration. In contrast, SEIK has the highest RMS error and the lowest Pearson correlation (PCC). This is mostly related to SEIK's stronger

Fig. 5 Seasonal variability of the mean 8-day Chl-a relative error (|data-model|/data) against the SeaWiFS Chl-a, averaged in the Adriatic Sea (*top left*), Gulf of Lions (*middle left*), Levantine basin (*bottom left*), Mediterranean (*bottom right*), and mean analysis (*top right*) and forecast (*middle right*) Chl-a relative error, averaged over the Mediterranean, for the simulations adopting the HYBRID (*red line*), SEIK (*black line*), SFEK (*green line*) assimilation filter schemes and the one without assimilation (FREE, *blue line*)

Mean Chl–a Relative Error (mean[|SeaWiFs−model|/SeaWiFs])
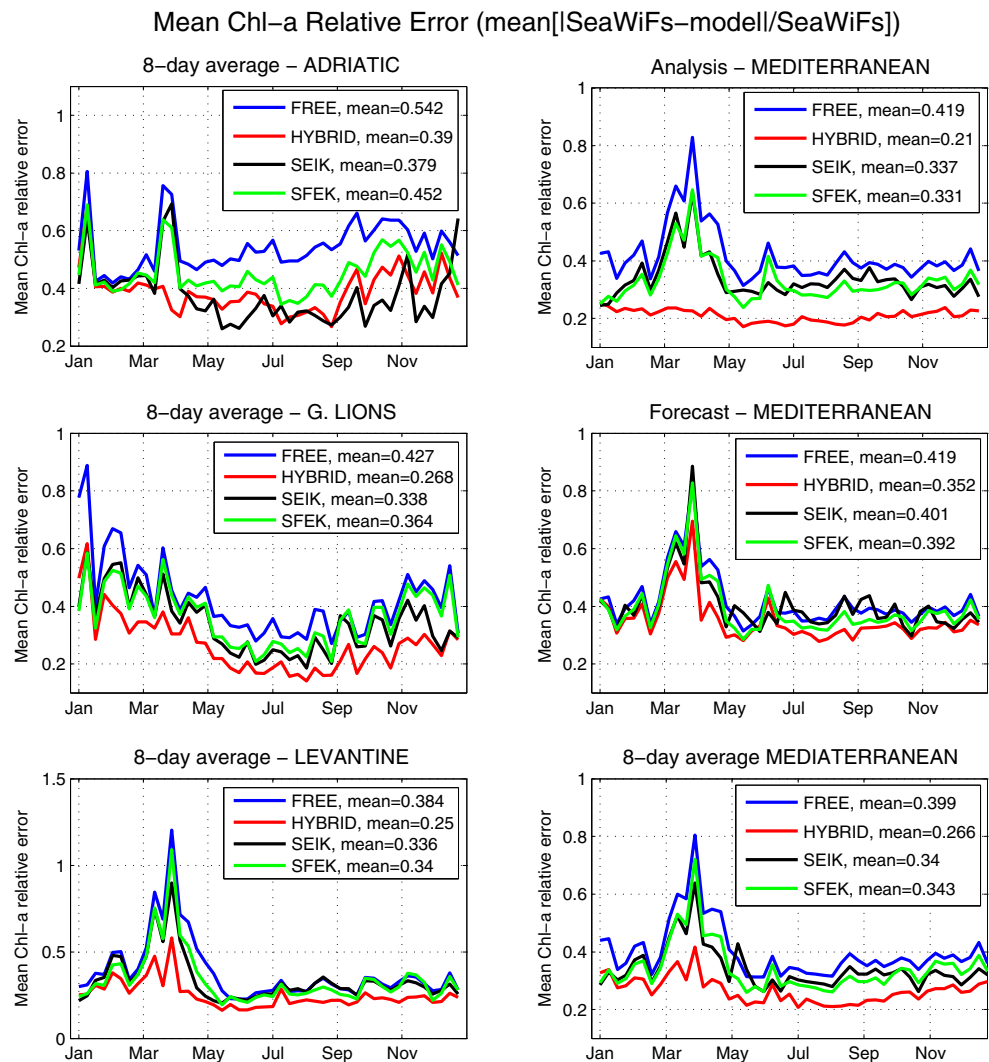
update in the productive Adriatic region (Figs. 4 and 5), where nutrient concentrations are highest. This stronger update results in a significant increase of nutrients that has a positive effect on PBIAS and STD, but a negative on model correlation and RMS error, suggesting a potential deterioration in reproducing the observed variability. When the Adriatic Sea is removed, the SEIK phosphate PBIAS is still better than HYBRID and SFEK, but differences are much lower. SEIK has also the lowest RMS error, indicating the good performance with phosphate. On the other hand, HYBRID leads to a higher correlation coefficient (with or without the Adriatic) and a lower RMS error, which are better indicators of the model performance, despite the weaker improvement in PBIAS and STD. In the case of nitrates, HYBRID improves both correlation and PBIAS, but slightly overestimates STD and has a higher RMS error. The simulation of nitrate is significantly deteriorated using SEIK, mainly due to its strong update in the Adriatic. In most of the Mediterranean,

phosphate is the main limiting factor for phytoplankton growth (Krom et al. 2004). This phosphate limitation is particularly noticeable in the Adriatic, which receives river nutrient loads characterized by high N:P ratios (Ludwig et al. 2009). Moreover, in this area, the model exhibits a systematic negative bias (Fig. 3). This is presumably due to an underestimation of phosphate river loads or also due to an overestimation of the retrieved Chl-a by the satellite bio-optical algorithm, as this may be influenced by land inputs of colored matter and suspended solids (Gregg and Casey 2004). Given this negative bias, the filter update results in an increase of nutrient concentrations, along with Chl-a. The addition of excess nitrogen that cannot be consumed by phytoplankton, being limited by phosphate, may result in nitrate built up by the model, as observed in the results of SEIK (see discussion below). The impact of SFEK on nitrate and phosphate is somewhat similar to HYBRID, as indicated by its skill indexes lying between HYBRID and the free-run.

5 Analysis of filters forecast update/spread and HYBRID sensitivity experiments

5.1 Forecast update

The impact of the different filtering schemes on Chl-a and dissolved inorganic nutrients is further investigated by examining the fractional change as imposed by the filters after the analysis step [FC = (analysis − forecast)/forecast] for Chl-a, phosphates and nitrates concentrations (Figs. 6 and 7). HYBRID leads to a much larger mean annual absolute fractional change (Fig. 6), particularly for Chl-a, indicating a more pronounced update as compared to SEIK and SFEK. It is noticeable that in the Adriatic, SEIK leads to a stronger change for nitrate and phosphate, as compared to HYBRID, despite the weaker correction it imposes on Chl-a. The more pronounced impact of SEIK on nitrates results in the overestimation mentioned above (Table 2). We should note, however, that nitrates updates are more significant, as compared to phosphates in all schemes. Areas showing a stronger update are those characterized by a larger model bias, such as the Adriatic, or those characterized by strong seasonal variability, such as the Gulf of Lions. SFEK imposes a relatively weaker

correction than both HYBRID and SEIK in the more productive areas, such as the Adriatic and G. Lions, but a slightly stronger correction than SEIK in more oligotrophic open sea areas, such as the Levantine basin. This differentiation in the filter's performance is related to the nature of their covariances. SEIK is more efficient in more productive and variable areas, such as the Adriatic and Gulf of Lions, due to its flow-dependent covariance, while SFEK shows a good performance in less variable areas, such as the Levantine, as its EOF-based covariance retains the spread of the dominant climatological modes of the system. HYBRID appears to perform well in all areas thanks to its "blended" covariance, estimated as a weighted average of flow-dependent and "smoothed" climatological covariances.

Figure 7 shows the different impacts of the filters on Chl-a, nitrates, and phosphates in the three focus areas: Adriatic, Gulf of Lions, and Levantine. In the Adriatic, SFEK mostly improves Chl-a, while SEIK imposes a more dynamically evolving update, based on its flow-dependent correction subspace, to all variables and in many cases most pronounced on nitrates. HYBRID improvement lies somewhere in between, leading to a stronger update of Chl-a, as SFEK, but with a more dynamically evolving
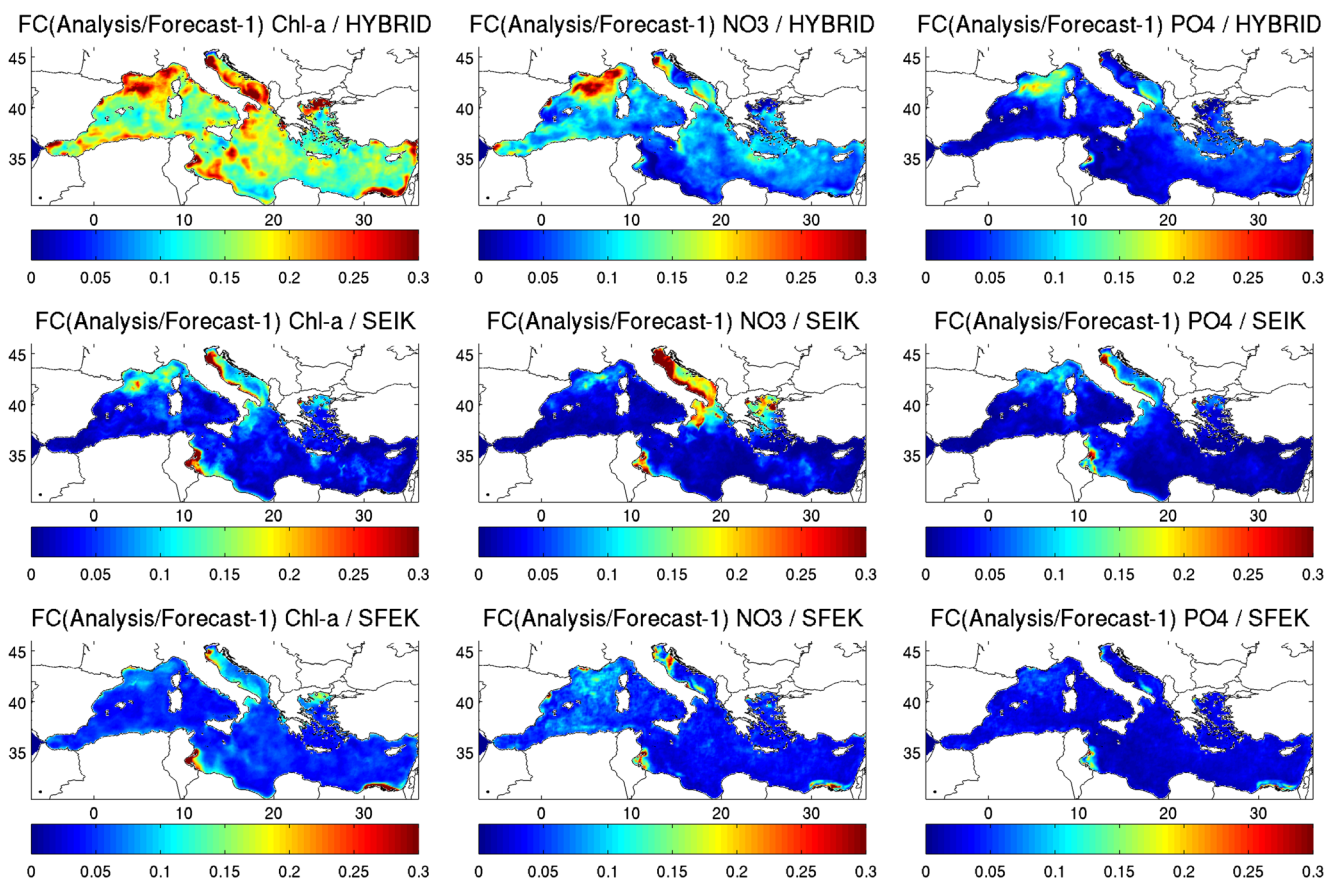
Fig. 6 Annual mean absolute fractional change (|Analysis-Forecast|/Forecast) of the Chl-a (*left column*), phosphates (*middle column*), and nitrates (*right column*) assimilation correction for HYBRID (*top*), SEIK (*middle*), and SFEK (*bottom*)

Table 2 Percentage bias (PBIAS), pearson correlation coefficient (PCC), normalized standard deviation [STDN = STD(model)/ STD(data)], and root mean square error (RMSE) of model simulated Chl (mg/m³), NO3 (mmol/m³), and PO4(mmol/m³) against SeaWiFS Chl-a and available in situ data over 1990–2009 period, collated from SeaDatanet database (www.seadatanet.org). The correlation coefficient is calculated on the logarithm of model and data values.

		PBIAS	PCC	STDN	RMSE
ChlSat (mg/m3)	Free	21.0	0.68	0.39	0.34
	Hybrid	19.1	0.84	0.38	0.32
	SEIK	15.7	0.82	0.53	0.30
	SFEK	19.4	0.78	0.38	0.33
PO4 (mmol/m3)	Free	35.0 (36.7)	0.34 (0.39)	0.30 (0.22)	0.0910 (0.092)
	Hybrid	33.5 (36.01)	0.35 (0.40)	0.30 (0.21)	0.0906 (0.0919)
	SEIK	28.1 (34.54)	0.32 (0.39)	0.44 (0.22)	0.0939 (0.0916)
	SFEK	34.9 (37.51)	0.34 (0.38)	0.30 (0.21)	0.0910 (0.0924)
NO3 (mmol/m3)	Free	18.4 (54.6)	0.277 (0.23)	1.09 (0.28)	3.29 (2.50)
	Hybrid	-1.8 (50.9)	0.279 (0.25)	1.30 (0.29)	3.61 (2.49)
	SEIK	-770.7 (-20.7)	0.178 (0.07)	27.15 (2.85)	64.91 (6.78)
	SFEK	3.3 (52.7)	0.2749 (0.23)	1.28 (0.28)	3.58 (2.49)

Values in parentheses are calculated excluding the Adriatic Sea (see Fig. 1). See section 2.3 for metrics definitions.

Red worse, *green* better

update and a stronger impact on other variables as in SEIK. The SEIK's stronger impact on phosphates (Figs. 6 and 7) results in a lower Chl-a error in the Adriatic, as compared to HYBRID (Fig. 5), despite its weaker impact on Chl-a. As nutrients are the driving fuel of phytoplankton, it appears to be more efficient for the filter to change those in order to achieve a better sustained change in phytoplankton. This information emerges from the statistics of flow-dependent covariance, as estimated from the evolving ensembles. A shortcoming of this dynamical behavior is that an inappropriate nutrients correction may lead to instabilities, as in the case of nitrates for SEIK. However, this is not entirely attributed to the filter. As explained above, phytoplankton growth is constrained by the most limiting nutrient and in most cases phosphates. The biogeochemical model provides a feedback to minimize the effect of an inappropriate correction of this limiting nutrient through its own dynamics, which is not the case for nitrates that are found in excess and are therefore susceptible to unconstrained instabilities. In that respect, HYBRID appears more robust than SEIK, as its dynamically based covariance is smoothed by a static one that was built by time-"smoothed" EOFs. In the Gulf of Lions, HYBRID imposes a stronger and more dynamically evolving update on all variables, as compared to SEIK and SFEK, showing peaks during the spring bloom events, which explains its more efficient error decrease (Figs. 3 and 5). In the Levantine, the filters impose a negative correction during the winter-spring period, to correct the model positive bias in this area (Figs. 2 and 3). This is most pronounced in HYBRID and comparable in SEIK and SFEK, as is the decrease of the respective errors (Fig. 5). During summer-autumn period, SFEK moderately changes Chl-a, while SEIK's update is quite weak for both Chl-a and nutrients, resulting in a weak error decrease (Figs. 3 and 5).

5.2 Ensemble spread

The poor performance of SEIK in the Eastern Levantine during the summer-autumn period (Figs. 5 and 7) can be related to the spread of the forecast ensemble

$(\delta X_a(t_k))$ that is calculated as the standard deviation of its ($N = 26$) ensemble members

$$\delta X^a(t_k) = \sqrt{\frac{1}{N} \sum_{i=1}^{N} \left[X_i^a(t_k) - \overline{X^a}(t_k) \right]^2} \qquad (14)$$

In the case of SFEK, the spread of the static ensemble is the standard deviation of the initial ensemble members ($\delta X_a(t_0)$), while in the case of HYBRID, the spread is calculated as a weighted combination ($\alpha = 0.95$) of the variance of the dynamic ($N_D = 10$) and static ($r_1 = 16$) ensemble.

As shown in Fig. 8, the spread of the SEIK ensemble for Chl-a in the Eastern Levantine significantly decreases after June, as is the correction imposed by the filter (Fig. 7). The opposite occurs in the Adriatic, where the SEIK ensemble exhibits a larger Chl-a spread, as compared to SFEK/HYBRID (Fig. 8), consistent with the SEIK smaller Chl-a error (Fig. 5). The HYBRID ensemble spread is quite close to the SFEK spread, due to the relatively

small (1-α = 0.05) contribution of the flow-dependent ensemble (this is the reason why the HYBRID ensemble spread is plotted on a different axis in Fig. 8, in order to better show its variability in time). In the Gulf of Lions, SEIK exhibits a slightly lower spread than SFEK/HYBRID, which is, however, maintained throughout the year, in contrast with the Eastern Levantine. The close relation between the SEIK ensemble spread and its ability to reduce the Chl-a estimation error can also be clearly identified, comparing the annual mean spread (Fig. 9) with the Chl-a relative error decrease (Fig. 4). One may notice that the areas where SEIK is more efficient are those characterized by a larger ensemble spread, such as the Adriatic, the North Aegean, and the Gulf of Lions. In contrast, areas where SEIK exhibits a poor performance, such as the coastal areas in the Eastern Levantine or the Alboran Sea, are those characterized by a smaller ensemble spread. In the Eastern Levantine, the small spread of the ensemble, particularly during summer-autumn periods (Fig. 8), can be attributed to the very low productivity (Fig. 2),
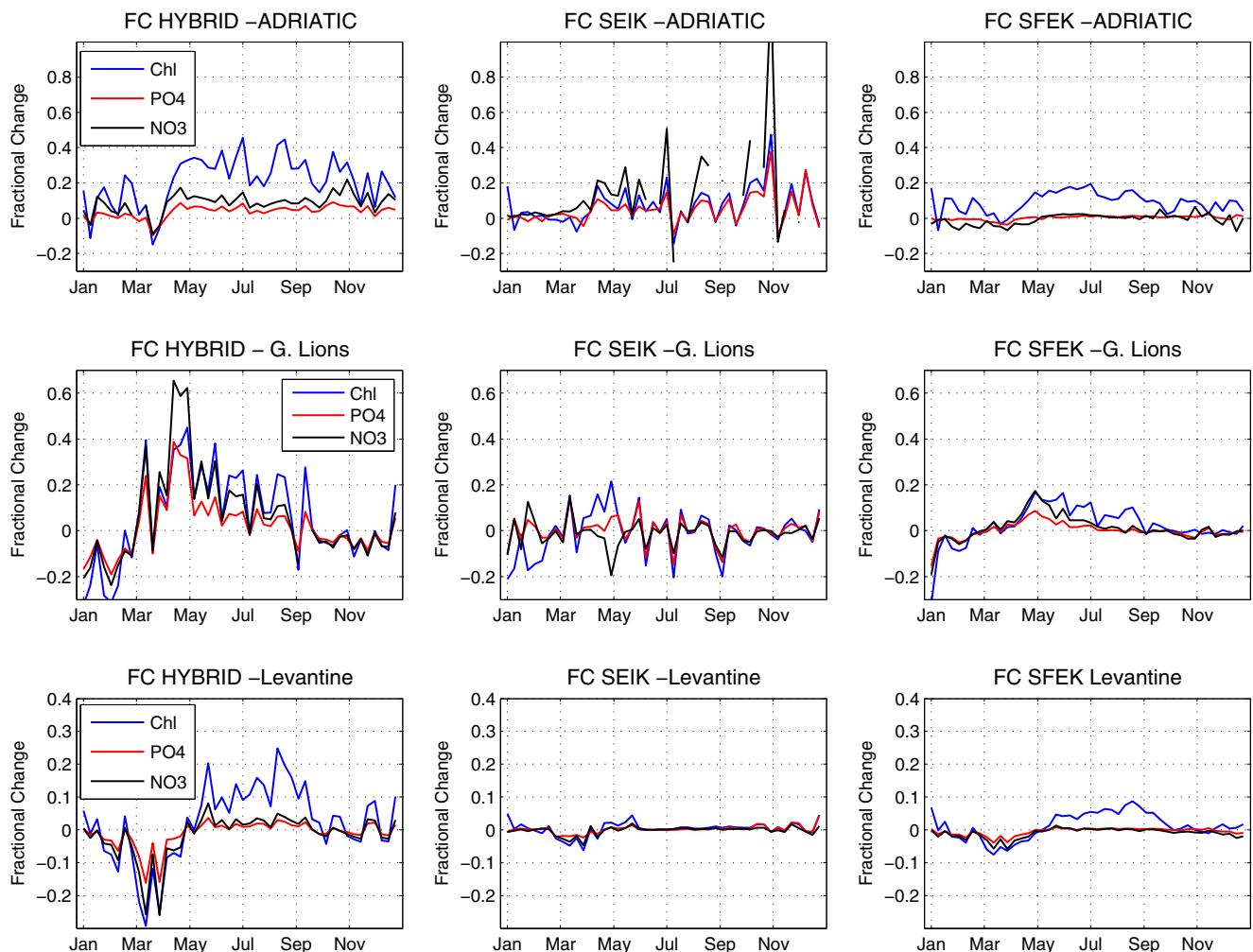
Fig. 7 Seasonal variability of the Chl-a (*blue line*), phosphates (*red line*), and nitrates (*black line*) assimilation correction fractional change (Analysis/Forecast-1) for HYDRID (*left column*), SEIK (*middle column*), and SFEK (*right column*), averaged over Adriatic (*top*), G. Lions (*middle*), and Levantine (*bottom*) areas
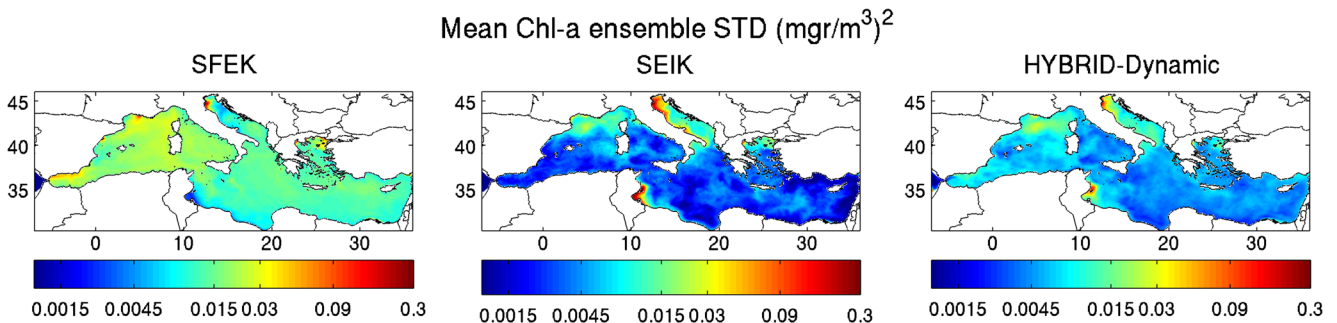
Fig. 8 Spread of Chl-a forecast ensemble (see Eq.14) for SEIK (*black line, left axis*), SFEK (*green line, left axis*), and HYBRID (*red line, right axis*), averaged over Adriatic, G.Lions and Levantine areas (Fig.1). The HYBRID spread (*red line*) is very close to SFEK and is also plotted on a different (*right*) axis in order to point out its variability with time
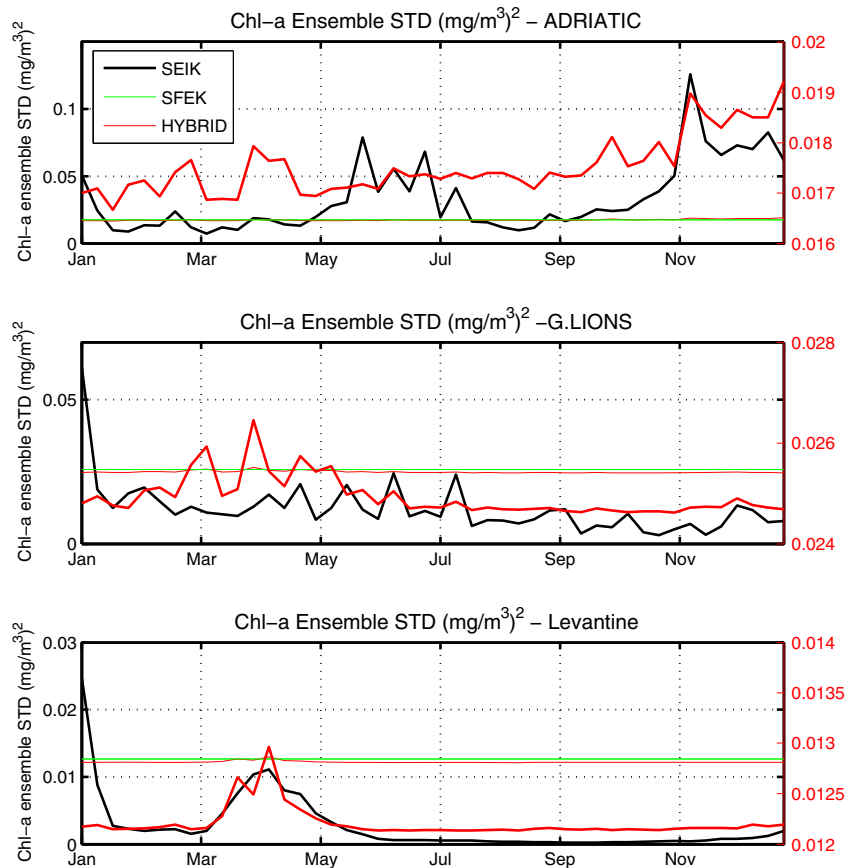
as surface nutrients are depleted, and Chl-a approaches very small values. On the other hand, the Alboran Sea is a productive and dynamic area, where one would expect a better performance for SEIK. The SEIK ensemble has enough spread in this area during the early assimilation window (not shown). However, the ensemble appears to have lost most of the initial spread after only few forecasting cycles with the model (Fig. 9). This may be attributed to the strong effect of circulation in this area, controlled by Atlantic water inflow and local atmospheric forcing that apparently drives the ensemble members closer to the mean state. One way to alleviate this could be to consider including stochastic perturbations in the model internal dynamics and/or the atmospheric forcing. A smaller

forgetting factor (i.e., larger inflation rate) should also result in a larger spread, but this would affect the entire domain. Given that in some areas, such as the Adriatic, SEIK already exhibits a sufficiently large spread and corrections, a spatially varying forgetting factor that would inflate the spread in areas where it is low, might be more appropriate (Anderson 2009).

A relatively small contribution ($1-\alpha = 0.05$) from the flow-dependent covariance is adopted in HYBRID (Eq. 11), resulting in an ensemble spread being effectively close to that of the SFEK static ensemble (Figs. 8 and 9). Including this small (5%) contribution from the flow-dependent covariance in HYBRID seems to significantly enhance the filter performance as compared to both SFEK and SEIK. As discussed in the next section, increasing the

Fig. 9 Annual mean spread of Chl-a forecast ensemble (see Eq.14) for SFEK (*left*), SEIK (*middle*), and HYBRID flow-dependent part (*right*). (The HYBRID total ensemble spread (Eq. 14) is very similar to that of SFEK)

weight of the flow-dependent covariance deteriorated the HYBRID behavior, which started resembling more the SEIK behavior, leading to an increased error for nitrates, particularly in the Adriatic (Table 2, see discussion in section 4.2). The relatively small (1-α = 0.05) flow-dependent contribution in HYBRID, that is found optimum in our case, is consistent with Counillon et al. (2009), who also found an optimum $\alpha = 0.95$ for their HYBRID scheme as compared to a 10-member ensemble Kalman filter and an Optimal Interpolation scheme. As mentioned above (section 4.2, Figs. 6–7), the HYBRID appears to impose a significantly stronger correction (Analysis-Forecast, Eq. 6) to the forecast, as compared to SFEK, despite their similar spread. Given that the HYBRID forecast error is always lower than SFEK (not shown), this stronger correction may be attributed to the more efficient representation of the error growth directions in the HYBRID covariance, which includes a flow-dependent component, allowing it to track changes in the system dynamics (Pham 2001; Hoteit et al. 2002; Hoteit et al. 2004). Another important attribute of HYBRID is its ability to maintain enough variance for its update step through the contribution of the static covariance. In this way, HYBRID remains efficient in areas, such as the Levantine, where SEIK ensemble members are driven to a similar state during summer, resulting in a poorer performance.

5.3 HYBRID sensitivity experiments

Another set of sensitivity experiments (see Table 1) was performed to investigate the sensitivity of the HYBRID scheme to the weighting factor and the size of the dynamically varying ensemble. In the reference HYBRID simulation (Table 1), the weighting parameter is $\alpha = 0.95$. When this is decreased to 0.7 and 0.5, i.e., assigning more weight to the flow-dependent ensemble covariance (see Eq. 11) in the analysis step, the Chl-a relative error is also decreased (Table 3), suggesting a more effective correction. However, in this case, HYBRID starts resembling more the SEIK behavior, increasing the nitrates correction in the Adriatic that results in a significant increase in the nitrate model bias.

The reference HYBRID simulation has used a flow-dependent ensemble of 10 members (Table 1). HYBRID was also tested with a flow-dependent ensemble of 5 (HYBRID_5), 15 (HYBRID_15), and 20 (HYBRID_20) members. The Chl-a mean relative error is slightly larger in HYBRID_5 simulation, but seems to quickly level off with an increasing flow-dependent ensemble size (Table 3). However, one may clearly notice that the larger flow-dependent ensemble results in an improvement of the Chl-a forecast, suggesting a more efficient projection of the Chl-a information onto the non-assimilated variables. A larger flow-dependent ensemble is therefore beneficial and is recommended depending on the availability of computational resources. HYBRID was not found sensitive to the rank of its static background covariance, providing very similar results to the reference HYBRID simulation (not shown), which is consistent with previous sensitivity experiments performed with SFEK (Hoteit et al. 2004).

6 Conclusions

A hybrid ensemble scheme, combining a flow-dependent ensemble covariance with a static background covariance, was developed and successfully implemented for assimilating satellite (SeaWiFS) Chl-a data into a marine ecosystem model of the Mediterranean. The performance of the new hybrid scheme (HYBRID) was assessed against a model free-run (without assimilation), and SEIK and SFEK schemes, with regard to the assimilated data (Chl-a) and non-assimilated model variables, such as dissolved inorganic nutrients (nitrates, phosphates).

The Chl-a estimation error against SeaWiFS significantly decreased after assimilation, particularly with the HYBRID scheme, correcting the most important model deficiencies. HYBRID reduced the error by more than 40% in most areas, as compared to the free-run, showing a slightly less pronounced improvement in the more productive areas, which could be explained by the relatively high observational error that has been adopted in these areas. SFEK estimation error exhibits similar patterns to that of

Table 3 Annual mean of 8-day average, analysis, and forecast relative Chl-a error (|data-model|/data), nitrates correction fractional change (FC, |analysis − forecast|/forecast), nitrates concentration in the Adriatic and nitrate overall model PBIAS, for different HYBRID runs (see also Table 1)

Blend parameter (a)	Size of evolving ensemble (r_k)	Chl-a R. error 8-day	Chl-a R. error forecast	Chl-a R. error analysis	NO3 FC	NO3 (mmol/m^3) Adriatic	NO3 PBIAS
0.95	5	0.273	0.3559	0.2077	0.15	0.67	0.74
0.95	10	0.266	0.352	0.21	0.11	0.69	−1.77
0.95	15	0.265	0.3513	0.2124	0.09	0.67	−1.44
0.95	20	0.264	0.3518	0.215	0.08	0.63	0.33
0.7	10	0.26	0.3493	0.2041	0.21	4.47	−90.64
0.5	10	0.262	0.3479	0.2093	0.24	8.75	−198.23

HYBRID, but is generally higher. SEIK leads to mixed performances, being more efficient than SFEK (and in some cases HYBRID) in more productive areas, and less efficient in others, mostly open-sea oligotrophic areas. This is related to the flow-dependent SEIK ensemble, efficiently identifying the directions of error growth in highly productive areas. In oligotrophic nutrient depleted areas during summer-autumn period, characterized by very low Chl-a, or in areas that are strongly controlled by circulation, the ensemble members are driven to a similar regime with small spread, leading to the SEIK poor performance.

The impact of data assimilation with the different filtering schemes on dissolved inorganic nutrients (phosphate, nitrate) was evaluated in terms of various skill indexes (bias, correlation, standard deviation, and RMS error), against a seasonal climatology (1990–1999) of in situ observations in the Mediterranean (SeaDataNet). Data assimilation had a positive overall impact on nutrients (as compared to the free-run) with regard to most skill indexes. An exception was the deterioration of nitrates simulation by SEIK in the Adriatic, which was related to its strong update in this productive area, and also to the phytoplankton limitation on phosphate that lead to a built up of excess of nitrates. SEIK, on the other hand exhibited a good performance, particularly in terms of mean model bias, with phosphate, which is the main limiting nutrient in the Mediterranean, thus, controlling primary production. HYBRID achieved the best and most robust performance improving phosphate, particularly in terms of correlation and RMS error, as well as nitrates, in terms of correlation and bias. The impact of SFEK on nitrate and phosphate was somewhat similar to HYBRID.

The filters different behavior was illustrated by the space-time variability of the forecast update on Chl-a and dissolved inorganic nutrients. SEIK imposed a more dynamically evolving correction that was in some cases stronger on nutrients, as compared to Chl-a. This emerges from the SEIK flow-dependent covariance, as nutrients effectively drive phytoplankton variability, and their change may result in a better sustained change in phytoplankton. A shortcoming of this behavior is that dynamical inconsistencies in the correction of nutrients may lead to instabilities, as in the case of nitrates in the Adriatic. SFEK appeared to have a stronger effect on Chl-a, while HYBRID in a way combines SFEK and SEIK attributes, leading to a stronger update for Chl-a, but with a more dynamically evolving update, based on its flow-dependent correction subspace and a stronger effect on other variables.

Adopting an increased contribution (weighting factor) from the flow-dependent covariance resulted in a more effective correction of Chl-a, but also in a deterioration of nitrates, similar to SEIK. An improvement in the HYBRID Chl-a forecast was also obtained with increased flow-dependent ensemble size, but this improvement in the filter performance quickly leveled off.

Overall, SEIK was found to be more efficient in more productive and variable areas, due to its flow-dependent covariance, while SFEK showed a better performance than SEIK in less variable areas, as its EOF-based covariance retains the main modes of the system long-term variability. HYBRID was more efficient than both SFEK and SEIK, as it appears to perform well in both types of areas, due to its "blended" covariance. Its flow-dependent component may track changes in the system dynamics, allowing for a more efficient representation of the error growth directions, which results in a better filter correction, even though the spread of its ensemble is largely determined by the static ensemble. Another important attribute of HYBRID is its ability to maintain a sufficient spread in its dynamic ensemble, thanks to its static covariance that mitigates the inbreeding of the ensemble.

Among the main challenges of assimilating satellite Chl-a in marine ecosystem models are the dynamically consistent projection of the Chl-a information onto non-assimilated variables, respecting the ecosystem dynamics, and the increased computational cost, given the large number of state variables. The developed hybrid assimilation scheme was found particularly robust and efficient in reducing the model Chl-a error but also showing a positive effect and dynamically consistent updates on non-assimilated variables. Moreover, its good performance with a relatively small flow-dependent ensemble size is translated to a significantly reduced computational load, which is particularly important for its operational implementation within the 3-D biogeochemical forecasting model of the Mediterranean. Future research besides an end-to-end ecosystem simulation analysis will also consider stochastic perturbation on the physical forcing and the ecosystem parameters, eventually developing and implementing filtering schemes for state parameter estimation.

References

Allen JI, Somerfield PJ, Siddorn J (2002) Primary and bacterial production in the Mediterranean Sea: a modelling study. J Mar Syst 33-34: 473–495. doi:10.1016/S0924-7963(02)00072-6

Allen JI, Eknes M, Evensen G, (2003) An Ensemble Kalman Filter with a complex marine ecosystem model: Hindcasting phytoplankton in the Cretan Sea. Annales Geophysicae 21(1):399–411

Anderson JL (2009) Spatially and temporally varying adaptive covariance inflation for ensemble filters. Tellus A 61:72–83

Azov Y (1991) Desert? Mar Pollut Bull 23:225–232

Barale V, Gade, M (Ed.) (2008) Remote sensing of the European seas. Springer Science+Business Media: Heidelberg. 22, pp. 514

Baretta JW, Ebenhoh W, Ruardij P (1995) The European regional seas ecosystem model, a complex marine ecosystem model. Neth J Sea Res 33:233–246

Blackford JC, Burkill PH (2002) Planktonic community structure and carbon cycling in the Arabian Sea as a result of monsoonalforcing: the application of a generic model. J Mar Syst 36(3–4):239–267

Blumberg AF, Mellor GL (1983) Diagnostic and prognostic numerical circulation studies of the South Atlantic Bight. J Geophys Res 88(C8):4579–4459

Bosc, E., Bricaud, A. et Antoine, D., (2004) Seasonal and interannual variability in algal biomass and primary production in the Mediterranean Sea, as derived from 4 years of SeaWiFS observations, Global Biogeochem Cycles, 18 (GB1005).

Brewin RJW, Dall'Olmo G, Pardo S, van Dongen-Vogels V, Boss ES (2016) Underway spectrophotometry along the Atlantic Meridional Transect reveals high performance in satellite chlorophyll retrievals. Remote Sens Environ 183:82–97. doi:10.1016/j.rse.2016.05.005

Ciavatta S, Torres R, Saux-Picart S, Allen JI (2011) Can ocean color assimilation improve biogeochemical hindcasts in shelf seas? J Geophys Res 116:C12043

Counillon F, Sakov P, Bertino L (2009) Application of a hybrid EnKF-OI to ocean forecasting. Ocean Sci 5:389–401

Dreano, D., Tandeo, P., Pulido, M., Ait-El-Fquih, B., Chonavelb, T., Hoteit, I. (2017) Estimating model error covariances in nonlinear state-space models using Kalman smoothing and the expectation-maximisation algorithm. Quarterly Journal of the Royal Meteorological Society, under minor revision.

Edwards C a, Moore AM, Hoteit I, Cornuelle BD (2015) Regional ocean data assimilation. Annu Rev Mar Sci 7:21–42. doi:10.1146/annurev-marine-010814-015821

Etherton BJ, Bishop CH (2004) Resilience of hybrid ensemble/3DVAR analysis schemes to model error and ensemble covariance error. Mon Weather Rev 132:1065–1080

Evensen G (2003) The ensemble Kalman filter: theoretical formulation and practical implementation. Ocean Dynam 53:343–367

Gharamti ME, Valstar J, Hoteit I (2014) An adaptive hybrid EnKF-OI scheme for efficient state-parameter estimation of reactive contaminant transport models. Adv Water Resour 71(1–15):2014

Gregg WW, Casey NW (2004) Global and regional evaluation of the SeaWiFS chlorophyll data set. Remote Sens Environ 93:463–479. doi:10.1016/j.rse.2003.12.012

Hamill TM, Snyder C (2000) A hybrid ensemble Kalman filter—3D variational analysis scheme. Mon Weather Rev 128:2905–2919

Hamill TM, Whitaker JS, Snyder C (2001) Distance-dependent filtering of background error covariance estimates in an ensemble Kalman filter. Mon Weather Rev 129:1790–2776

Horton C, Clifford M, Schmitz J, Kantha LH (1997) A real-time oceanographic nowcast/forecast system for the Mediterranean sea. J Geophys Res 102(C11):25123–25156

Hoteit I, Pham D-T (2004) An adaptively reduced-order extended Kalman filter for data assimilation in the tropical Pacific. J Mar Syst 45:173–188

Hoteit I, Pham DT, Blum J (2001) A semi-evolutive partially local filter for data assimilation. Mar Pollut Bull 43:164–174

Hoteit I, Pham DT, Blum J (2002) A simplified reduced order Kalman filtering and application to altimetric data assimilation in Tropical Pacific. J Mar Syst 36:101–127

Hoteit I, Triantafyllou G, Petihakis G, Allen JI (2003) A singular evolutive extended Kalman filter to assimilate real in situ data in a 1-D marine ecosystem model. Ann Geophys. doi:10.5194/angeo-21-389-2003

Hoteit I, Triantafyllou G, Petihakis G (2004) Towards a data assimilation system for the Cretan Sea ecosystem using a simplified Kalman filter. J Mar Syst 45:159–171

Hoteit I, Triantafyllou G, Petihakis G (2005) Efficient data assimilation into a complex, 3-D physical-biogeochemical model using partially-local Kalman filters. Ann Geophys 23:3171–3185

Hoteit I, Luo X, Pham D-T (2012) Particle kalman filtering: a nonlinear bayesian framework for ensemble kalman filters. Mon Weather Rev 140(2):528–542

Hoteit I, Hoar T, Gopalakrishnan G, Collins N, Anderson J, Cornuelle B, Köhl A, Heimbach P, Kohl A, Heimbach P (2013) A MITgcm/DART ensemble analysis and prediction system with application to the Gulf of Mexico. Dyn Atmos Ocean 63:1–23. doi:10.1016/j.dynatmoce.2013.03.002

Hu J, Fennel K, Mattern JP, Wilkin JL (2012) Data assimilation with a local Ensemble Kalman Filter applied to a three-dimensional biological model of the Middle Atlantic Bight. J Mar Syst 94:145–156

Jolliff, J., Kindle, J., Shulman, I., (2009) Summary diagrams for coupled hydrodynamic- ecosystem model skill assessment JMar Sys 76, 64–82. http://dx.doi.org/10.1016/ j.jmarsys.2008.05.014

Kalaroni S, Tsiaras K, Petihakis G, Hoteit I, Economou-Amilli A, Triantafyllou G (2016) Data assimilation of depth-distributed satellite chlorophyll-α in two Mediterranean contrasting sites. J Mar Syst 160:40–53. doi:10.1016/jmarsys.2016.03.018

Korres G, Lascaratos A (2003) An eddy resolving model of the Aegean and Levantine basins for the Mediterranean Forecasting System Pilot Project (MFSPP): implementation and climatological runs. Ann Geophys 21:205–220

Korres G, Hoteit I, Triantafyllou G (2007) Data assimilation into a Princeton Ocean Model of the Mediterranean Sea using advanced Kalman filters. J Mar Syst 65:84–104. doi:10.1016/j.jmarsys.2006.09.005

Krom M, Herut B, Mantoura CFR (2004) Nutrient budget for the Eastern Mediterranean: implications for phosphorus limitation. Limnol Oceanogr 49:1582–1592

Lenartz F, Raick C, Soetaert K, Grégoire M (2007) Application of an Ensemble Kalman filter to a 1-D coupled hydrodynamic-ecosystem model of the Ligurian Sea. J Mar Syst 68(3–4):327–348

Li H, Kalnay E, Miyoshi T (2009) Simultaneous estimation of covariance inflation and observation errors within an ensemble Kalman filter. QJR Meteorol Soc 135:523–533. doi:10.1002/qj.371

Ludwig, W., .Dumont, E., Meybeck, M., Heussner, S., (2009) River discharges of water and nutrients to the Mediterranean and Black Sea: major drivers for ecosystem changes during past and future decades? Prog Oceanogr 80: 199–217

Lui B, Ait-El-Fquih B, Hoteit I (2016) Efficient Kernel-based ensemble Gaussian mixture filtering. Mon Wea Rev 144:781–800

Luo X, Bhakta T (2016) Estimating observation error covariance matrix of seismic data from a perspective of image denoising. Comput Geosci. doi:10.1007/s10596-016-9605-0

Macias D, Guerreiro CT, Prieto L, Peliz A, Ruiz J (2014) A high-resolution hydrodynamicbiogeochemical coupled model of the Gulf of Cadiz - Alboran Sea region. Mediterr Mar Sci 15(4):739–752

Marty J, Chiavérini J, Pizay M, Avril B (2002) Seasonal and interannual dynamics of nutrients and phytoplankton pigments in the western Mediterranean Sea at the DYFAMED time-series station (1991–1999). Deep-Sea Res II Top Stud Oceanogr 49:1965–1985

Mellor GL, Yamada T (1982) Development of a turbulence closure model for geophysical fluid problems. Rev Geophys 20:851–875. doi:10.1029/RG020i004p00851

Miyoshi T, Kalnay E, Li H (2013) Estimating and including observation-error correlations in data assimilation. Inverse Problems in Science and Engineering 21(3):387–398

Morel A, André J-M, Andre J-M (1991) Pigment distribution and primary production in the western Mediterranean as derived and modeled from coastal zone color scanner observations. J Geophys Res. doi:10.1029/95JC00466

Moutin T, Raimbault P (2002) Primary production, carbon export and nutrients availability in western and eastern Mediterranean Sea in early summer 1996 (MINOS cruise). J Mar Syst 33-34:273–288. doi:10.1016/S0924-7963(02)00062-3

Nerger L, Danilov S, Hiller W, Schroter J (2006) Using sea-level data to constrain a finite-element primitive-equation ocean model with a local SEIK filter. Ocean Dynam 56:634–649

Nerger L, Gregg WW (2007) Assimilation of SeaWiFS data into a global ocean-biogeochemical model using a local SEIK filter. J Mar Syst 68:237–254. doi:10.1016/j.jmarsys.2006.11.009

Nittis K, Perivoliotis L, Korres G, Tziavos C, Thanos I (2006) Operational monitoring and forecasting for marine environmental applications in the Aegean Sea. Environ Model Softw 21:243–257

O'Reilly JE, Maritorena S, Mitchell BG, Siegel DA, Carder KL, Garver SA, Kahru M, Reilly MO, Maritorena JE, Mitchell S, Siegel BG, Carder DA, Garver KL, Kahru SA, McClain C (1998) Ocean color chlorophyll algorithms for SeaWiFS. J Geophys Res 103:24937. doi:10.1029/98JC02160

Papadopoulos A, Kallos G, Katsafados P, Nickovic S (2002) The Poseidon weather forecasting system: an overview. The Global Atmosphere and Ocean Systems 8:219–237 (retitled Journal of Atmospheric and Ocean Science).

Pätsch J, Radach G (1997) Long-termsimulation of the eutrophication of the North Sea: temporal development of nutrients, chlorophyll and primary production in comparison to observations. J Sea Res 1101

Petihakis G, Triantafyllou G, Allen IJ, Hoteit I, Dounas C (2002) Modelling the spatial and temporal variability of the Cretan Sea ecosystem. J Mar Syst 36(3–4):173–196

Petihakis G, Tsiaras K, Triantafyllou G, Kalaroni S, Pollani A (2014) Sensitivity of the N. Aegean Sea ecosystem to Black Sea Water inputs Mediterr Mar Sci:790–804

Pham D (2001) Stochastic methods for sequential data assimilation in strongly nonlinear systems. Mon Weather Rev:1194–1207

Simon E, Bertino L (2009) Application of the Gaussian anamorphosis to assimilation in a 3-D coupled physical-ecosystem model of the North Atlantic with the EnKF: A twin experiment. Ocean Sci 5(4):495–510

Song H, Hoteit I, Cornuelle BD, Subramanian AC (2010) An adaptive approach to mitigate background covariance limitations in the ensemble Kalman filter. Mon Weather Rev 138(7):2825–2845

Stow, C.a., Jolliff, J., McGillicuddy, D.J., Doney, S.C., Allen, J.I., Friedrichs, M.A.M., Rose, K.A., Wallhead, P., (2009) Skill assessment for coupled biological/physical models ofmarine systems. J Mar Syst 76, 4–15. http://dx.doi.org/10.1016/j.jmarsys.2008.03.011

Teruzzi A, Dobricic S, Solidoro C, Cossarini G (2014) A 3-D variational assimilation scheme in coupled transport-biogeochemical models: Forecast of Mediterranean biogeochemical properties. J Geophys Res Ocean 119:200–217. doi:10.1002/2013JC009277

Triantafyllou G, Hoteit I, Petihakis G (2003) A singular evolutive interpolated Kalman filter for efficient data assimilation in a 3D complex physical-biogeochemical model of the Cretan Sea. J Mar Syst 40-41:213–231

Triantafyllou G et al (2005) Ecosystem modeling and data assimilation of physical-biogeochemical processes in shelf and regional areas of the Mediterranean Sea. App Num Anal Comp Math 2:262–280

Triantafyllou G et al (2007) Assimilation of ocean colour data into a Biochemical Flux Model of the Eastern Mediterranean Sea. Ocean Sci 3:397–410

Triantafyllou G, Yao F, Petihakis G et al (2014) Exploring the Red Sea seasonal ecosystem functioning using a three-dimensional biophysical model. J Geophys Res-Oceans 119:1791–1811. doi:10.1002/2013jc009641

Tsiaras, K., Korres, G., Petihakis, G., Nittis, K., Raitsos, D., Pollani A., Triantafyllou, G., (2010) The Poseidon ecosystem model: the Mediterranean case. Proceedings of the 5th International Conference of EuroGOOS, EuroGOOS publication n. 28, ISBN 978–91–974828-6-8: 191–198.

Tsiaras KP, Petihakis G, Kourafalou VH, Triantafyllou G (2014) Impact of the river nutrient load variability on the North Aegean ecosystem functioning over the last decades. J Sea Res 86:97–109. doi:10.1016/j.seares.2013.11.007

Tugrul S, Besiktepe ST, Salihoglou I (2002) Nutrient exchange fluxes between the Aegean and Black Seas through the Marmara Sea. Mediterr Mar Sci 3:33–42

Ueno G, Nakamura N (2014) Iterative algorithm for maximum-likelihood estimation of the observation-error covariance matrix for ensemble-based filters. Q J R Meteorol Soc 140(678):295–315

Wang X, Barker DM, Snyder C, Hamill TM (2008) A hybrid ETKF-3DVAR data assimilation scheme for the WRF model. Part II: real observation experiments. Mon Weather Rev 136:5132–5147

Whitaker JS, Hamill TM (2002) Ensemble data assimilation without perturbed observations. Weather Rev 130:1913–1924

Xu FH, Oey LY, Miyazawa Y, Hamilton P (2013) Hindcasts and forecasts of Loop Current and eddies in the Gulf of Mexico using local ensemble transform Kalman filter and optimum-interpolation assimilation schemes. Ocean Model 69:22–38

Zavatarelli M, Mellor GL (1995) A numerical study of the Mediterranean Sea circulation. J Phys Oceanogr 25(6):1384–1414